



Method for localizing intraoperative recordings from deep brain stimulation surgery using post-operative structural MRI

McKenzie Winter^a, Jamie D. Costabile^b, Aviva Abosch^b, John A. Thompson^{b,*}

^a Department of Cell and Developmental Biology, Modern Human Anatomy, United States

^b Department of Neurosurgery, University of Colorado School of Medicine, Aurora, CO, United States

ABSTRACT

Background: Implantation of deep brain stimulation (DBS) electrodes for the treatment of involuntary movement disorders, such as Parkinson's disease, routinely relies on the use of intraoperative electrophysiological confirmation to identify the optimal therapeutic target in the brain. However, only a few options exist to visualize the relative anatomic localization of intraoperative electrophysiological recordings with respect to post-operative imaging. We have developed a novel processing pipeline to visualize intraoperative electrophysiological signals registered to post-operative neuroanatomical imaging.

New method: We developed a processing pipeline built on the use of ITK-SNAP and custom MATLAB scripts to visualize the anatomical localization of intraoperative electrophysiological recordings mapped onto the post-operative MRI following implantation of DBS electrodes. This method combines the user-defined relevant electrophysiological parameters measured during the surgery with a manual segmentation of the DBS electrode from post-operative MRI; mapping the microelectrode recording (MER) depths along the DBS lead track.

Results: We demonstrate the use of our processing pipeline on data from Parkinson's disease patients undergoing DBS implantation targeted to the subthalamic nucleus (STN). The primary processing components of the pipeline are: extrapolation of the lead wire and alignment of intraoperative electrophysiology.

Conclusion: We describe the use of a processing pipeline to aid clinicians and researchers engaged in deep brain stimulation work to correlate and visualize the intraoperative recording data with the post-operative DBS trajectory.

1. Introduction

Deep brain stimulation (DBS) is a common therapy for the motor symptoms of Parkinson's disease (PD) (Benabid et al. 2009). Standard practice for DBS implantation at many institutions worldwide relies on intraoperative microelectrode recordings (MER) to delineate single-neuron responses corresponding to voluntary and passive motor tasks, increasing efficacy in localizing the therapeutic target (Abosch et al. 2013). In current practice, few centers have access to tools that would permit visual confirmation of intraoperative electrophysiology - used to infer brain anatomy - co-registered to post-operative structural MR (magnetic resonance) anatomy.

Intraoperative single and multi-unit microelectrode recordings remain a dominant method for implantation of electrodes into the ventral intermediate thalamus for essential tremor, subthalamic nucleus or globus pallidus internus (GPI) for Parkinson's disease (PD), and GPI for dystonia (Bari et al. 2018). However, validation or confirmation of intraoperative MER electrophysiology is often overlooked in post-surgical analysis due to the lack of available tools. Many sophisticated tools exist for post-operative representation of the DBS lead in

normalized MNI (Montreal Neurological Institute) space (Butson et al. 2011, 2007; Chaturvedi et al. 2010; D'Haese et al. 2012; Horn et al. 2017; Horn and Kühn 2015; Pallavaram et al. 2008), using automated extraction of the DBS lead - particularly using post-operative computed tomography (CT) (Husch et al. 2018) - which may not accurately represent electrode curvature and thus fail to show correspondence with intraoperative recording locations. In addition, limited options exist for aligning the intraoperative electrophysiology with post-operative imaging in patient native MRI space.

This study illustrates a processing pipeline for visualizing agreement between inferred anatomy from electrophysiological signals and post-operative MRI. This processing suite uses the manually extracted 3D model of the DBS lead, from a post-operative MR imaging set, to extrapolate the recording trajectories of the implanted track and any additional recording tracks relative to a standard neurosurgical microelectrode holder. Registered to post-operative MR, computed single-neuron parameters (e.g., firing rate) are aligned along their respective recording trajectories. Post-surgical evaluation of intraoperative electrophysiology parameters in relation to their putative recording trajectories within post-operative MR space, typically used for

* Corresponding author at: University of Colorado School of Medicine, Department of Neurosurgery, RC2 Rm # 5119, 12800 E. 19th Ave., Aurora, CO 80045, United States.

E-mail address: john.a.thompson@ucdenver.edu (J.A. Thompson).

<https://doi.org/10.1016/j.nicl.2018.10.016>

Received 31 January 2018; Received in revised form 10 October 2018; Accepted 16 October 2018

Available online 16 October 2018

2213-1582/ © 2018 The Authors. Published by Elsevier Inc. This is an open access article under the CC BY-NC-ND license (<http://creativecommons.org/licenses/by-nc-nd/4.0/>).

determination to determine a well-placed DBS lead, will permit post-operative confirmation of inferred anatomy and assist in DBS related research.

2. Methods

2.1. Subjects

For this study, data were derived from three subjects undergoing DBS (3389; Medtronic, Minneapolis, MN) implantation surgery targeted to the STN for the treatment of PD (3 males; age 58.7 ± 1.5 years; mean \pm STD; 2 right hemisphere implantations). All subjects met accepted selection criteria for STN-DBS, including a persistent positive response to anti-PD medications ($> 30\%$ improvement on the motor subscale of the Unified Parkinson's Disease Rating Scale, in the on- vs. off-state (Abosch et al. 2012)), the absence of dementia on neuropsychological testing, and medical clearance for surgery.

2.2. Imaging acquisition

For this study we used a pre-operative non-contrast 3D T1 volumetric scan and a post-operative T2-weighted or susceptibility-weighted scan, both acquired on a 1.5 T MRI (Siemens, Symphony Magnetom TIM – 8 channel). The bottom of contact 0 was identified in the axial plane, as the first ventral slice with the absence of electrode artifact in the T2 sequence (see Fig. 1 A, C for example images).

2.3. MNI registration

To visualize the electrophysiological parameter of interest in MNI-152 standard atlas space we used a linear rigid transformation of the post-operative T2 with the ICMB152-T2 (provided in the supplementary material along with the ICMB152-T1; <http://nist.mni.mcgill.ca/?p=798>; Mazziotta et al., 2001a) in ITK-SNAP. Briefly, using ITK-SNAP, the post-operative T2 sub-cortical slab (dimensions: $512 \times 512 \times 35$ pixels; $0.5 \times 0.5 \times 2$ mm; see Fig. 4A), was registered to the ICMB152-T2 using a rigid transformation with mutual information as the image similarity metric. The transform matrix resulting from the registration was applied to the electrode mask. Finally, both the transformed NIFTI files (electrode mask and post-operative T2) were resliced with a z-dimension matching the ICMB152-T2 sequence.

2.4. Data preprocessing

Processing steps are diagrammed in Fig. 2. The first step in preparing the MR neuroimaging data requires removing voxels that represent non-brain tissue, such as skull and scalp features. To complete this process, within the Mango (Multi-Image Analysis GUI; <http://ric.uthscsa.edu/mango/>; (Kochunov et al., 2002), we applied the Brain Extraction Tool (BET) from the FSL neuroimaging analysis suite (Smith 2002) to both the pre-operative T1 and post-operative T2. To extract a binary mask of the DBS lead, axial T2-weighted post-operative MRI were used to identify the location of the wire artifact. The DBS lead of interest (i.e., Left or Right) was manually segmented using ITK-SNAP (www.itksnap.org; (Yushkevich et al. 2006)). The manually segmented

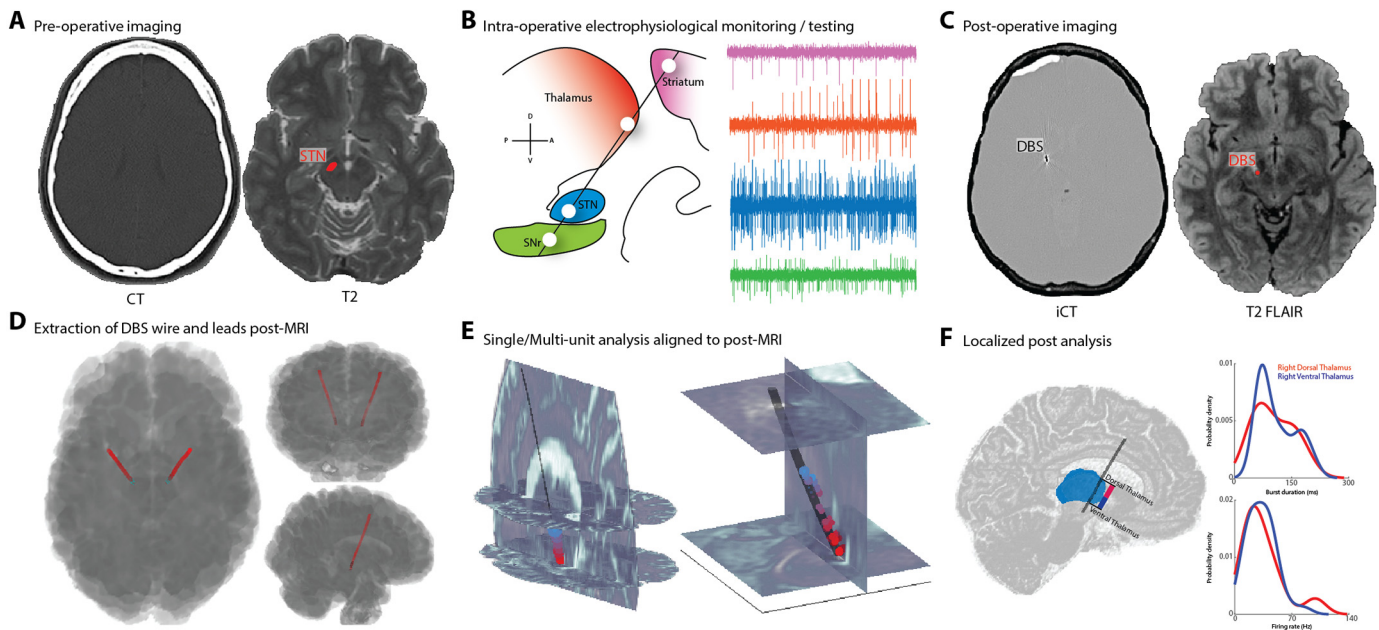


Fig. 1. A, For the deep brain implantation procedure, pre-operative stereotactic neuronavigation planning involves the acquisition of a computed tomography (CT) sequence set for reducing susceptibility to image distortion, in addition a structural T1 magnetic resonance image data set (standard volumetric voxel size: $1 \times 1 \times 1 \text{ mm}^3$) is often collected to register frame-based and non-frame based stereotactic systems. Finally, specific MRI sequences may be obtained to enhance identification of the intended target (e.g., T2-FLAIR for the subthalamic nucleus (STN)). B, Intraoperative verification of the intended DBS target for implantation to treat movement disorders may involve correlating kinesthetic responses with single neuron electrophysiology (i.e., microelectrode recordings). The left panel highlights the common brain structures traversed during implantation of the STN. In the right panel, color-coded voltage traces illustrate the unique electrophysiological signatures associated with each brain structure. C, Post-operative imaging for DBS usually entails acquisition of a CT sequence (iCT indicates an grayscale inverted CT image to enhance the visualization of the DBS electrode) set to assess presence and extent of edema due to recording and implantations tracts. In addition, an MRI sequence set is acquired to verify placement of the DBS electrode. D, We have developed a method to permit manual extraction of the DBS electrode from post-operative MRI. The panel highlights the 3D model of the bilateral DBS electrodes in the Axial (left panel), Coronal (top right), and Sagittal (bottom right). E, Further, our analysis will provide the capability to overlay intraoperative electrophysiological parameters collected during surgery in register with the 3D modeled DBS electrode aligned with the pre- or post-operative MRI data sequences. The left panel is zoomed out image of the implanted electrode highlighting dorsal (blue) and ventral (red) recordings with STN. F, Analyses of electrophysiological parameters can be directly visualized with the pre- or post-operative MRI space. Population quantification of the dorsal and ventral thalamus recordings (left panel) are represented for burst duration (top right) and firing rate (bottom right).

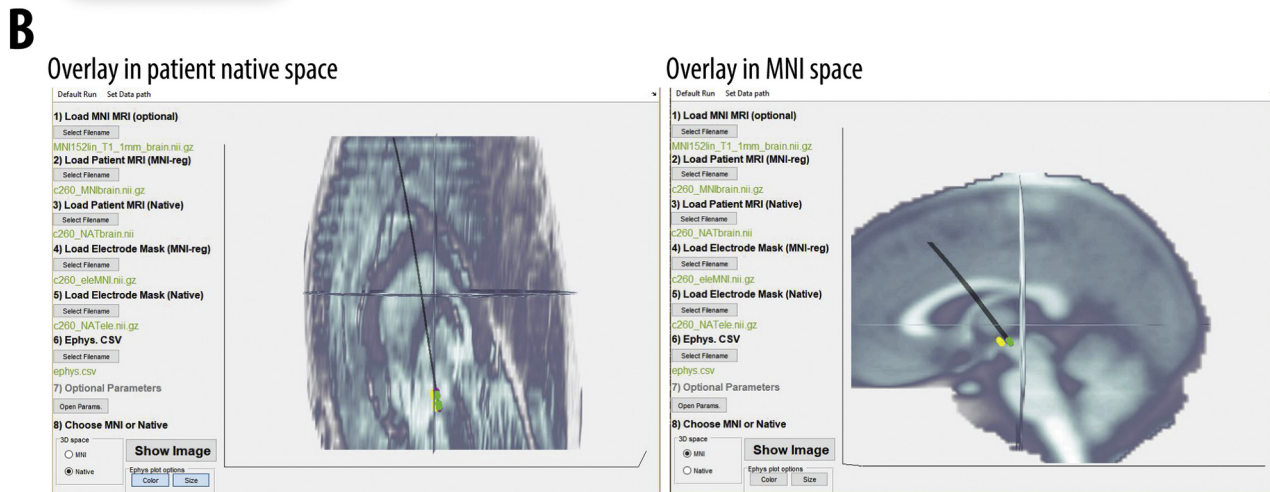
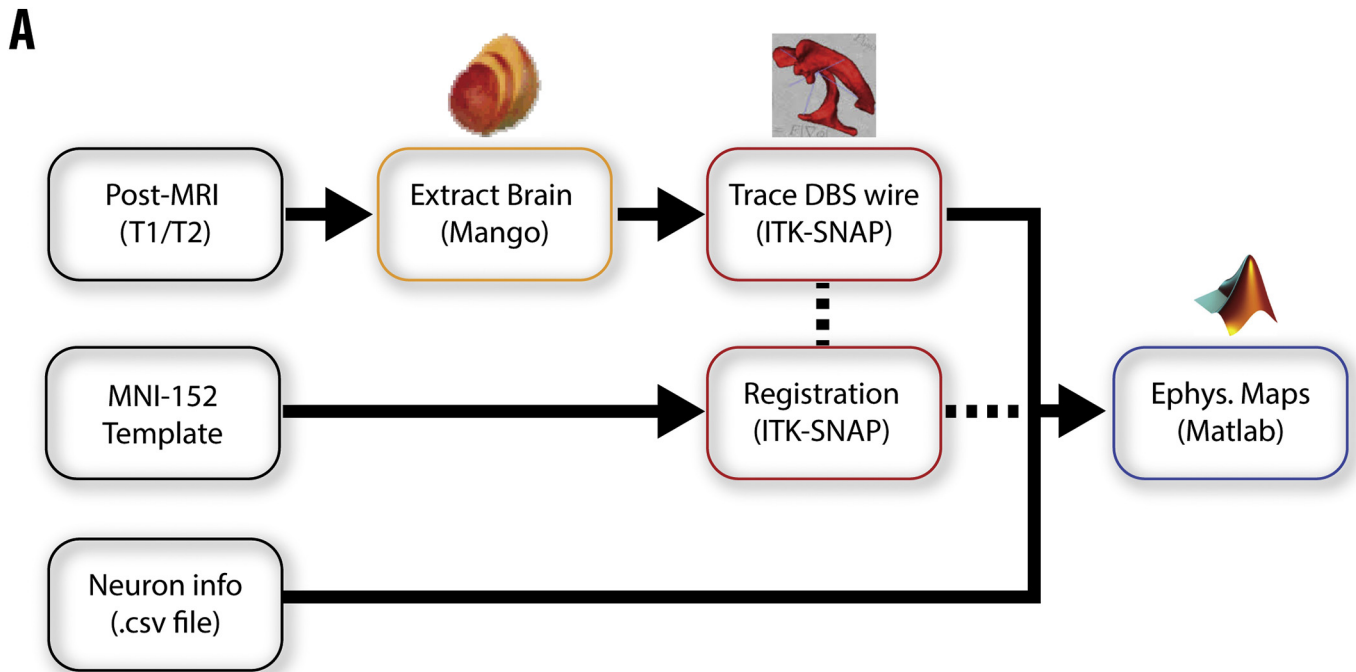


Fig. 2. A, Flow diagram for the sequence of programs used in the pre-processing of the neuroimaging data. First, all pre and post-operative image datasets were converted into NIFTI file format and then skull-stripped using the FSL Brain Extraction Tool as a plugin within the Mango neuroimaging suite. Next, the DBS wire was manually traced in the post-operative imaging sequence and exported as binary mask using the ITK-SNAP neuroimaging analysis suite. These data were then imported into MATLAB to map and align the intraoperative electrophysiological data. B, GUI application example views of native space post-operative MRI with electrophysiological parameter overlay (top) and the electrophysiological data registered to the MNI space (bottom).

3D polygon composite of the DBS electrode was exported from ITK-SNAP as a binary mask. The transformation matrix computed from the registration of the T2 to the T1 was applied to the 3D binary mask of the DBS electrode.

2.5. Electrode modeling

The processing steps involved in generating a model of the DBS lead based on the manually derived binary mask were executed using custom programs written in MATLAB 2016b (Mathworks, Natick, MA). Fig. 3 represents the transformation of the manually traced DBS segmentation to a processed mesh occurring within MATLAB. All MATLAB functions associated with this procedure are available <https://github.com/neuropil/DBS-NP-Map>. In addition to base MATLAB, the following toolboxes are required to use our pipeline: Imaging Processing, Curve Fitting, and Statistics and Machine Learning. The DBS electrode processing program (ExtractDBSPolygon.m), reads in the binary mask (.nii)

using the NIFTI Tool box suite (file exchange). First, for each axial plane, the centroid and area are computed for the 2D binary map representing the electrode mask (Fig. 4 B2). Next, the array representing the centroids derived from the 3D plane stack is interpolated with a 1-D spline function and smoothed using a robust version of a local regression with weighted linear least squares and a 2nd degree polynomial model (i.e., MATLAB function ‘*rloess*’). The original number of slice planes in the z-dimension (i.e., axial plane) are re-sampled from the smoothed and interpolated centroid array. Finally, at each axial plane, a new binary mask is computed to represent the electrode mask. The new mask is represented by a circle centered on the new centroid and is computed with the diameter of the actual DBS electrode lead (e.g., Medtronic 3389: ~1.3 mm).

2.6. Electrophysiological mapping

For this study, we collected microelectrode recordings using either a

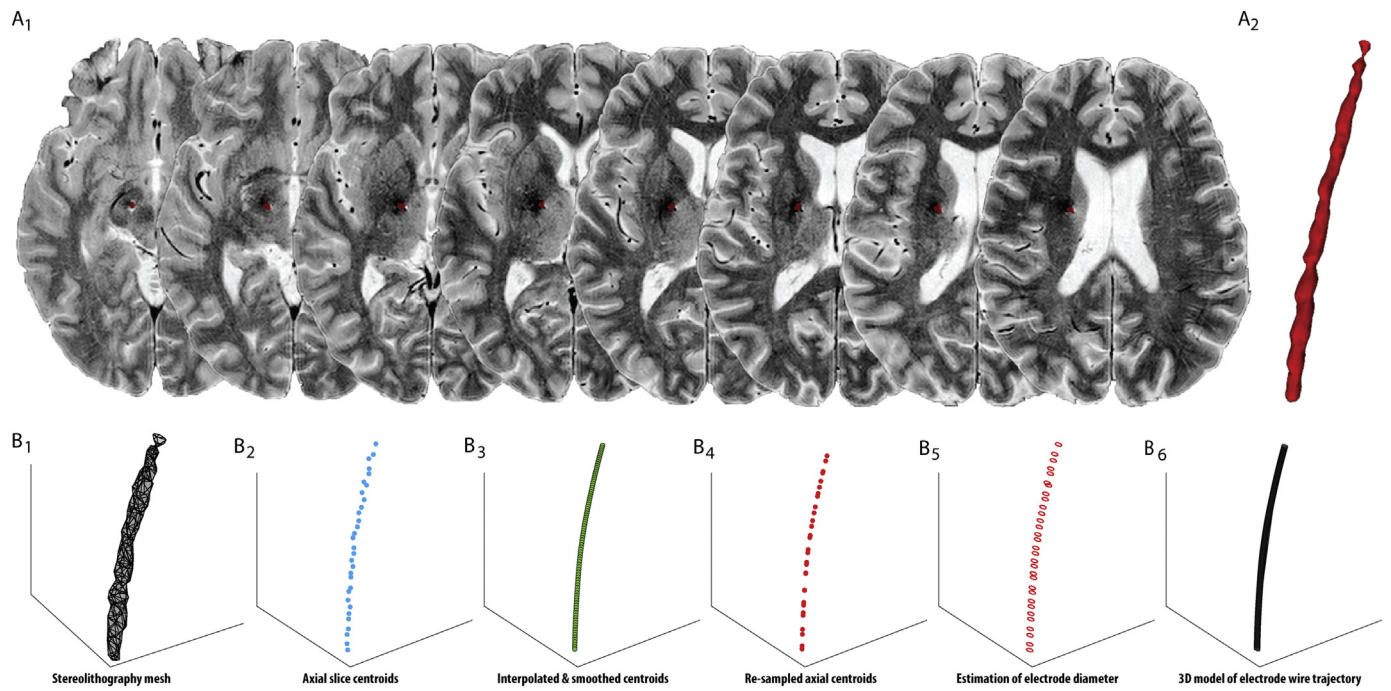


Fig. 3. *A₁*, Axial sections from a post-operative T2 FLAIR MRI, following DBS implantation, in which the subthalamic nucleus (STN) has been manually traced with an enclosed region-of-interest (ROI; red polygon). The polygons were traced onto each section using ITK-SNAP. *A₂*, 3D polygon rendering of the concatenated 2D traced polygons created within ITK-SNAP. *B₁*, The ITK-SNAP 3D model of the DBS electrode is imported and visualized in MATLAB using the ‘patch’ function to render the vertices and faces of the polygon. *B₂*, The centroid of the 2D polygon within each axial slice is estimated. *B₃*, The estimated centroid locations are interpolated in the z-axis and smoothed (using a Savitzky-Golay moving average filter) in the x, y and z axis. *B₄*, The new centroids are re-sampled at the original z-axis dimensions to maintain the original MRI 3D space parameters. *B₅*, From the revised centroids, new polygon radii are estimated based on the actual diameter of the implanted electrode and extension wire. *B₆*, Representation of the final 3D render of the extracted DBS wire.

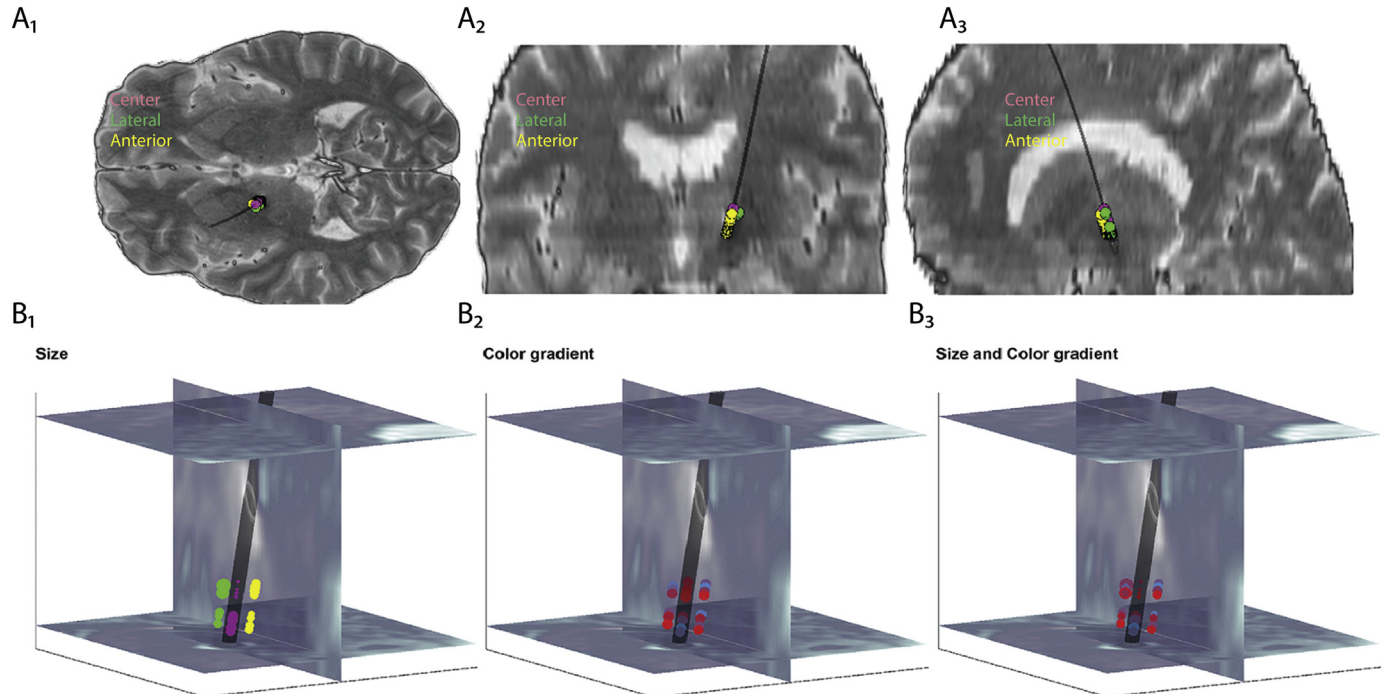


Fig. 4. *A₁*, Representative example, in the axial plane, for overlying the electrophysiological recording locations from three simultaneous microelectrode recordings onto the pre-operative T1 MRI (center, lateral and anterior reflect the recording locations with respect to the microelectrode guide posts on the BenGun). Each bubble indicates a unique intraoperative recording location. The black cylinder depicts the 3D representation of the electrode wire. *A₂*, Coronal perspective for the same representative example in *A₁*. *A₃*, Sagittal perspective for the same representative example in *A₁*. *B₁₋₃*, Three representative examples depicting post-operative alignment of electrophysiological single recording data with native space T2 MRI.

MicroGuide or NeuroOmega electrophysiological recording system (AlphaOmega, Nazareth, Israel). Our analysis was not dependent upon the recording system, and our software was not dependent on a specific neurophysiological software processing suite. To align a selected single or multi-neuron electrophysiological metric (e.g., firing rate) with the 3D model of the DBS lead within the post-operative MR space we used the following procedure. The neurophysiological metrics required for the alignment process include the following for each recording location contained in a Microsoft Excel file or comma delimited file (i.e., .csv): 1) neurophysiological parameter of interest (e.g., normalized root mean square of the voltage amplitude, number of individual neurons, average firing rate of single neurons, etc.), 2) electrode number, which is the arbitrary number assigned to the electrode with the BenGun microelectrode holder (permits the use of up to 5 electrodes), 3) trajectory orientation relative to BenGun microelectrode holder position (e.g., center, anterior, posterior, lateral, or medial), 4) recording depth relative to the assigned stereotactic target (i.e., 0 mm). The recording depth was encoded in micrometers in an integer format (see supplemental example datasheet SM1.csv). All recording depth values encoded by the neurophysiological system were normalized relative to the last recording value by computing their difference. The current version of the program was developed using clinical recordings generated by an Alpha Omega clinical electrophysiology system, which outputs recording depth values estimated in millimeters. These values were referenced to the z-axis of the 3D DBS model within the post-operative MR space based on the slice and voxel dimensions of the MRI (DeriveXYZ_NeurOverlay.m). The difference in distance between the last recording depth and the recording depth of interest is added to the bottom depth value computed from the DBS wire model in MR space to derive the recording position in MR space. To obtain the optimal MR depth index, a k-nearest neighbor analysis is applied to the available MR depth values and the computed recording depth value. For the k-nearest neighbor analysis, the interpolated, sub-millimetric MR depth values are used to provide greater resolution of the optimal recording depth value approximation. In addition to the MATLAB functions, we have provided a GUI ('DBS_PostMR_IORecording.fig; <https://github.com/neuropil/DBS-NP-Map>) application for ease of interaction with the visualization features (see Manual in supplementary materials for use), see Fig. 2B for a representation of the user interface. In addition, there is a main function that will generate the entire processing suite and can be used in isolation (DisplayEphys2DBS.m).

2.7. Post-operative electrophysiological mapping

The electrophysiological feature intended for post-operative representation can be reflected within MR space using two image properties to indicate relative differences across recording depths. Relative differences in the electrophysiological property as a function of depth can be displayed using either size or a color gradient. To generate this representation, the values are normalized to the maximum value of the input feature vector (e.g., firing rate). However, it is also feasible to plot the locations of the recording information within the available recording trajectories without any relative difference in magnitude.

3. Results

3.1. Electrode mapping visualization

The primary use of this software suite is the visualization of intraoperative single or multi-unit neurophysiological data collected from the implantation of a DBS wire in post-operative MR imaging. Fig. 4A1-3 shows an example of intraoperative recording locations aligned with a 3D manually extracted model of the DBS electrode along with extrapolated MER trajectories derived from the post-operative MRI. In the example surgery displayed in the panel, there were three simultaneous microelectrode recording trajectories – center, anterior, and lateral –

depicted by different colors.

The second feature permits the visualization of relative differences in the single or multi-unit physiological parameter of interest as a function of depth. The relative difference in magnitude can be visualized either by the scaled size of the circle or bubble used to represent each depth (like a bubble chart; see Fig. 4 B1) or the difference in a binary color gradient with the polar color extremes representing the highest and lowest values (see Fig. 4 B2). These features can also be combined (see Fig. 4 B3).

4. Discussion

4.1. Mapping electrophysiology to the DBS electrode in post-operative MRI

We have demonstrated the use of a novel processing pipeline for DBS electrode implantation by registering anatomical localization of intraoperative electrophysiological recordings onto post-operative MRI. Current literature predominately relies on post-operative CT extraction of the DBS electrode wire and stimulating contacts to assess DBS placement. Post-operative CT imaging does not include anatomical data thus requiring atlas registration to the extracted DBS leads. Secondly some institutions solely acquire post-operative MRIs. These institutions are limited by current literature in evaluating DBS lead placement due to incompatibility between imaging modality and available analysis algorithms. Our study addresses these constraints by developing a visualization pipeline using post-operative MRI in mapping intraoperative electrophysiology to the DBS electrode. Various electrophysiological variables used during intraoperative implantation could be viewed post-operatively for post-hoc confirmation; these variables could include the following: normalized root mean square (NRMS) of the MER, firing rate of identified single neurons, burst profile, and local field potential mean power for a specific frequency band (Moran et al. 2006; Valsky et al. 2017; Zaidel et al. 2009). NRMS has been used for the identification of STN (Valsky et al. 2017), firing rate of individual neurons used to distinguish between commonly traversed structures (Gross et al. 2006), and LFP power which may assist with identification of the optimal stimulation target within STN (Zaidel et al. 2010). The selection of electrophysiological parameters will depend on the outcome of interest, which may depend on identification of the functional territory activated during surgery, or localization of a structure based on characteristic activity patterns.

4.2. Applications

DBS is used to treat many medical conditions in addition to Parkinson's, including ET, dystonia, and OCD (Miocinovic et al. 2013). Intertwining scientific research with surgical intervention, DBS is proving to have new indications in treating other neurologic and behavioral diseases including depression, schizophrenia, Alzheimer's, and obesity (Greenberg et al. 2010; Mann et al. 2017). As research continues expanding our understanding of subcortical electrophysiological functions and associated treatment applications, the neurosurgical community will require tools in overlaying and validating intraoperative electrophysiology (Udupa et al. 2015). Our analysis pipeline provides opportunity in expanding applications to DBS electrophysiology of other subcortical targets. Additionally, the following algorithms highlight the areas of subcortical recordings and allow direct visualization of these parameters aligned with the post-operative MRI.

4.3. Limitations

Our pipeline does not provide a robust DBS electrode extraction function, and it is a significant limitation that our extraction protocol requires manual segmentation. The objective for our extraction method was constructed for use in cases where post-operative CT was not

available as well as in cases where the post-operative MRI were acquired with low resolution sequence parameters. However, our program will accept a mesh binary map for the DBS electrode wire derived from another algorithm or application.

Conflict of interest

The authors declare no conflicts of interests.

Acknowledgements

This research was supported by funds from the Boettcher Foundation's Webb-Waring Biomedical Research Awards program.

Appendix A. Supplementary data

Supplementary Figure – Function flow chart. Diagram representing the organization of the custom MATLAB functions, with descriptions for input and output arguments, used to execute the visualization. Supplementary data to this article can be found online at <https://doi.org/10.1016/j.nicl.2018.10.016>.

References

- Abosch, A., Lanctin, D., Onaran, I., Eberly, L., Spaniol, M., Ince, N.F., 2012. Long-term recordings of local field potentials from implanted deep brain stimulation electrodes. *Neurosurgery* 71, 804–814. <https://doi.org/10.1227/NEU.0b013e3182676b91>.
- Abosch, A., Timmermann, L., Bartley, S., Rietkerk, H.G., Whiting, D., Connolly, P.J., Lanctin, D., Hariz, M.I., 2013. An international survey of deep brain stimulation procedural steps. *Stereotact. Funct. Neurosurg.* 91, 1–11. <https://doi.org/10.1159/000343207>.
- Bari, A.A., Thum, J., Babayan, D., Lozano, A.M., 2018. Current and Expected advances in Deep Brain Stimulation for Movement Disorders. *Prog. Neurol. Surg.* 33, 222–229. <https://doi.org/10.1159/000481106>.
- Benabid, A.L., Chabardes, S., Mitrofanis, J., Pollak, P., 2009. Deep brain stimulation of the subthalamic nucleus for the treatment of Parkinson's disease. *Lancet Neurol.* 8, 67–81. [https://doi.org/10.1016/S1474-4422\(08\)70291-6](https://doi.org/10.1016/S1474-4422(08)70291-6).
- Butson, C.R., Cooper, S.E., Henderson, J.M., Wolgamuth, B., McIntyre, C.C., 2011. Probabilistic analysis of activation volumes generated during deep brain stimulation. *NeuroImage* 54, 2096–2104. <https://doi.org/10.1016/j.neuroimage.2010.10.059>.
- Chaturvedi, A., Butson, C.R., Lempka, S.F., Cooper, S.E., McIntyre, C.C., 2010. Patient-specific models of deep brain stimulation: Influence of field model complexity on neural activation predictions. *Brain Stimul.* 3, 65–77. <https://doi.org/10.1016/j.brs.2010.01.003>.
- D'Haese, P.-F., Pallavaram, S., Li, R., Remple, M.S., Kao, C., Neimat, J.S., Konrad, P.E., Dawant, B.M., 2012. CranialVault and its CRAVE tools: a clinical computer assistance system for deep brain stimulation (DBS) therapy. *Med. Image Anal.* 16, 744–753. <https://doi.org/10.1016/j.media.2010.07.009>.
- Greenberg, B.D., Rauch, S.L., Haber, S.N., 2010. Invasive circuitry-based neurotherapeutics: stereotactic ablation and deep brain stimulation for OCD. *Neuropsychopharmacology* 35, 317–336. <https://doi.org/10.1038/npp.2009.128>.
- Gross, R.E., Krack, P., Rodriguez-Oroz, M.C., Reza, A.R., Benabid, A.L., 2006. Electrophysiological mapping for the implantation of deep brain stimulators for Parkinson's disease and tremor. *Mov. Disord.* 21. <https://doi.org/10.1002/mds.20960>.
- Horn, A., Kühn, A.A., 2015. Lead-DBS: a toolbox for deep brain stimulation electrode localizations and visualizations. *NeuroImage* 107, 127–135. <https://doi.org/10.1016/j.neuroimage.2014.12.002>.
- Horn, A., Neumann, W.-J., Degen, K., Schneider, G.-H., Kühn, A.A., 2017. Toward an electrophysiological “sweet spot” for deep brain stimulation in the subthalamic nucleus. *Hum. Brain Mapp.* 00. <https://doi.org/10.1002/hbm.23594>.
- Husch, A., V Petersen, M., Gemmar, P., Goncalves, J., Hertel, F., 2018. PaCER - a fully automated method for electrode trajectory and contact reconstruction in deep brain stimulation. *NeuroImage: Clin.* 17, 80–89. <https://doi.org/10.1016/j.nicl.2017.10.004>.
- Mann, A., Gondard, E., Tampellini, D., Milsted, J.A.T., Marillac, D., Hamani, C., Kalia, S.K., Lozano, A.M., 2017. Chronic deep brain stimulation in an Alzheimer's disease mouse model enhances memory and reduces pathological hallmarks. *Brain Stimul.* <https://doi.org/10.1016/J.BRS.2017.11.012>.
- Miocinovic, S., Somayajula, S., Chitnis, S., Vitek, J.L., 2013. History, applications, and Mechanisms of Deep Brain Stimulation. *JAMA Neurol.* 70, 163. <https://doi.org/10.1001/2013.jamaneurol.45>.
- Moran, A., Bar-Gad, I., Bergman, H., Israel, Z., 2006. Real-time refinement of subthalamic nucleus targeting using Bayesian decision-making on the root mean square measure. *Mov. Disord.* 21, 1425–1431. <https://doi.org/10.1002/mds.20995>.
- Pallavaram, S., D'Haese, P.-F., Kao, C., Yu, H., Remple, M., Neimat, J., Konrad, P., Dawant, B., 2008. A new method for creating electrophysiological maps for DBS surgery and their application to surgical guidance. Springer, Berlin, Heidelberg, pp. 670–677. https://doi.org/10.1007/978-3-540-85988-8_80.
- Smith, S.M., 2002. Fast robust automated brain extraction. *Hum. Brain Mapp.* 17, 143–155. <https://doi.org/10.1002/hbm.10062>.
- Udupa, K., Ghahremani, A., Chen, R., 2015. Are we close to the advent of closed loop deep brain stimulation in Parkinson's disease? *Mov. Disord.* 30, 1326. <https://doi.org/10.1002/mds.26343>.
- Valsky, D., Marmor-Levin, O., Deffains, M., Eitan, R., Blackwell, K.T., Bergman, H., Israel, Z., 2017. Stop! border ahead: automatic detection of subthalamic exit during deep brain stimulation surgery. *Mov. Disord.* 32, 70–79. <https://doi.org/10.1002/mds.26806>.
- Yushkevich, P.A., Piven, J., Hazlett, H.C., Smith, R.G., Ho, S., Gee, J.C., Gerig, G., 2006. User-guided 3D active contour segmentation of anatomical structures: significantly improved efficiency and reliability. *NeuroImage* 31, 1116–1128. <https://doi.org/10.1016/j.neuroimage.2006.01.015>.
- Zaidel, A., Spivak, A., Shpigelman, L., Bergman, H., Israel, Z., 2009. Delimiting sub-territories of the human subthalamic nucleus by means of microelectrode recordings and a Hidden Markov Model. *Mov. Disord.* 24, 1785–1793. <https://doi.org/10.1002/mds.22674>.
- Zaidel, A., Spivak, A., Grieb, B., Bergman, H., Israel, Z., 2010. Subthalamic span of oscillations predicts deep brain stimulation efficacy for patients with Parkinson's disease. *Brain* 133, 2007–2021. <https://doi.org/10.1093/brain/awq144>.